

DTP/96/102
 RAL-TR-96-103
 December 1996
 (revised January 1997)

Consistent Treatment of Charm Evolution in Deep Inelastic Scattering

A. D. Martin^a, R. G. Roberts^b, M. G. Ryskin^{a,c} and W. J. Stirling^{a,d}

^a *Department of Physics, University of Durham, Durham, DH1 3LE*

^b *Rutherford Appleton Laboratory, Chilton, Didcot, Oxon, OX11 0QX*

^c *Laboratory of Theoretical Nuclear Physics, St. Petersburg Nuclear Physics Institute,
 Gatchina, St. Petersburg 188350, Russia*

^d *Department of Mathematical Sciences, University of Durham, Durham, DH1 3LE*

Abstract

We present a formulation which allows heavy quark (c, b, \dots) mass effects to be explicitly incorporated in both the coefficient functions and the splitting functions in the parton evolution equations. We obtain a consistent procedure for evolution through the threshold regions for $c\bar{c}$ and $b\bar{b}$ production in deep inelastic scattering, which allows the prediction of the charm and bottom quark densities. We use the new formulation to perform a next-to-leading order global parton analysis of deep inelastic and related hard scattering data. We find that the optimum fit has $\alpha_S(M_Z^2) = 0.118$. We give predictions for the charm components of the proton structure functions F_2 and F_L as functions of x and Q^2 and, in particular, find that F_2^c is in good agreement with the existing measurements. We examine the Q^2 range of validity of the photon-gluon fusion model for $c\bar{c}$ electroproduction. We emphasize the value of a precision measurement of the charm component F_2^c at HERA.

1. Introduction

A very wide range of deep inelastic scattering structure function data can be successfully described in terms of universal quark and gluon distributions satisfying DGLAP (Q^2) evolution equations. While the formalism for light quarks (i.e. $m_q \ll \Lambda_{QCD}$) is on a sound theoretical footing, the treatment of heavy quarks (i.e. $m_q \gg \Lambda_{QCD}$) is more problematic. The reason is that in practice one requires a consistent description which includes both the kinematical regions $Q^2 \sim m_q^2$ and $Q^2 \gg m_q^2$.

The problem of how to treat heavy quark contributions to deep inelastic structure functions has been widely discussed, see for example [1]. It has been brought into focus recently by the very precise $F_2^{ep}(x, Q^2)$ data from HERA. Both the H1 and ZEUS collaborations have measured [2, 3] the charm quark component F_2^c of the structure function at small x and have found it to be a large (approximately 25%) fraction of the total. This is in sharp contrast to what is found at large x , where typically $F_2^c/F_2 \sim O(10^{-2})$ [4]. Since the HERA F_2 data [5, 6] are a potentially valuable source of information on the gluon distribution, the value of α_S , and the relation between the non-perturbative (low Q^2) and perturbative (high Q^2) domains, it is important that charm component is treated correctly.

In this paper we present a new, theoretically consistent method for calculating the heavy quark contributions to the deep inelastic electroproduction structure functions F_2 and F_L .¹ Our main focus is on the charm quark contribution, although our results apply equally well for bottom and top quarks. The most important feature of our analysis is that it is applicable both to the threshold region $Q^2 \sim 4m_c^2$, where phase space effects are important, and to the asymptotic region $Q^2 \gg 4m_c^2$, where the charm quark assumes the role of a massless parton and the DGLAP resummation of leading $(\alpha_S \ln Q^2)^n$ contributions is necessary.

Before describing our formalism and presenting quantitative predictions, we briefly review existing techniques for treating the charm quark contribution to F_2 . The most simplistic approach is to assume that a probe of virtuality Q^2 can resolve a charm quark pair in the proton sea when $Q^2 \gtrsim m_c^2$. Since such pairs originate from fluctuations of the gluon field, $g \rightarrow c\bar{c}$, a perturbative treatment should be valid as long as $m_c^2 \gg \Lambda_{QCD}^2$. As Q^2 increases, $O(m_c^2/Q^2)$ corrections to the standard DGLAP evolution become less important, and the charm quark can be treated as a (fourth) massless quark. These ideas are embodied in the ‘massless parton evolution’ (MPE) approach

$$\begin{aligned} c(x, Q^2) &= 0 \quad \text{for} \quad Q^2 \leq \mu_c^2, \\ n_f &= 3 + \theta(Q^2 - \mu_c^2) \quad \text{in} \quad P_{qg}, P_{gg}, \beta_0, \dots, \end{aligned} \tag{1}$$

where $\mu_c = O(m_c)$. The charm contribution to the structure function is then

$$F_2^c(x, Q^2) = \frac{8}{9}xc(x, Q^2) \tag{2}$$

¹Note that we only consider here the case of neutral current deep inelastic scattering. The case of charged current scattering, e.g. $W^-c \rightarrow s$, will be somewhat different but can in principle be treated using the same techniques.

in lowest order. This is the approach adopted at NLO in the MRS (and CTEQ) global parton analyses, with μ_c chosen to achieve a satisfactory description of the EMC F_2^c data [4]. For example, in the MRS(A) analysis [7] it was found that $\mu_c^2 = 2.7 \text{ GeV}^2$ and that this was to a good approximation equivalent to taking

$$2c(x, Q_0^2) = \delta \mathcal{S}(x, Q_0^2) \quad (3)$$

with $\delta \approx 0.02$ at the input scale $Q_0^2 = 4 \text{ GeV}^2$. That is at the input scale, charm ($c + \bar{c}$) was found to have approximately the same shape as the total quark sea distribution \mathcal{S} , and moreover to form about 2% of its magnitude. The input parameter μ_c^2 (or equivalently δ) was chosen to give a good description of the EMC F_2^c data.

Although phenomenologically successful, the MPE model clearly cannot give a precise description of the charm contribution in the threshold region. Two-body kinematics imply that an on-shell $c\bar{c}$ pair can be created by photon-gluon fusion (PGF) provided

$$W^2 = Q^2 \frac{1-x}{x} \geq 4m_c^2 \quad (4)$$

where W is the $\gamma^* g \rightarrow c\bar{c}$ centre-of-mass energy. That is, at small x , $c\bar{c}$ production is not forbidden even at small $Q^2 < \mu_c^2$ where the MPE approach gives zero². In the PGF approach, which was used, for example, in refs. [9, 10, 11], F_2^c is calculated using the exact matrix elements and phase space for the process $\gamma^* g \rightarrow c\bar{c}$. In leading order in α_S we have

$$F_2^c(x, Q^2) = \int dz C_g(z, Q^2, \mu^2) \frac{x}{z} g\left(\frac{x}{z}, \mu^2\right). \quad (5)$$

Note that the scale μ^2 at which the gluon distribution and the coupling α_S (in the coefficient function C_g) are evaluated is not specified at leading order, but one might guess that $\mu^2 = O(m_c^2)$ is appropriate. We discuss a reasonable choice of μ^2 in more detail in section 3 together with the effects coming from next-to-leading order (NLO) corrections. In contrast to the situation for massless quarks, there is no collinear divergence in the leading-order $\gamma^* g \rightarrow c\bar{c}$ calculation: the integral over the transverse momentum of the produced $c\bar{c}$ pair is regulated by the quark mass: $\int dk_T^2 k_T^2 / (k_T^2 + m_c^2)^2$. However, this in turn means that at very high Q^2 the leading-order contribution behaves as $F_2^c \sim \alpha_S(\mu_c^2) \ln(Q^2/m_c^2)$. Higher-order corrections also behave as $(\alpha_S \ln(Q^2/m_c^2))^n$, and fixed-order perturbation theory breaks down. In fact these large logarithms are precisely those which are resummed by the DGLAP evolution equations. Thus at large Q^2 we have to include the charm quark as a parton in DGLAP evolution. The exact next-to-leading order corrections to the PGF structure function are known [12]. Indeed very recently [13] this leading-twist analysis has been used to perform $(\alpha_S \ln(Q^2/m_c^2))^n$ resummation for $Q^2 \gg m_c^2$. However such an approach is of course not applicable in the threshold region $Q^2 \gtrsim m_c^2$, which we also wish to study because of the HERA data for F_2 in this domain.

²In ref. [8] the MPE model was modified by the introduction of a smooth ‘smearing’ function which gave a gradual onset of the charm distribution from a low input scale Q_0^2 , namely $Q_0^2 = 1 \text{ GeV}^2$.

Our goal is to include the charm quark in parton evolution in a consistent way. First, in section 2, we discuss how to include the heavy quark mass in the Altarelli-Parisi splitting kernels in such a way as not to destroy the original parton interpretation, that is to ensure energy-momentum conservation etc. In order to be consistent with the $\overline{\text{MS}}$ factorization scheme the threshold for the onset of the charm distribution is $Q^2 = m_c^2$. Although in fact we will see that charm partons cannot be resolved in the timescale ($\Delta t \sim 1/\Delta E \sim 2E/Q^2$) of the fluctuations of the gluon into a $c\bar{c}$ pair until $Q^2 > 4m_c^2$. In section 3 we discuss the coefficient functions. The PGF contribution will be included in the coefficient function for the gluon distribution. Thus below the resolution threshold of the charm distribution, $Q^2 < 4m_c^2$, our result for $c\bar{c}$ production will not be zero but will agree with the PGF approach. However, at large Q^2 , as was noted in ref. [14], part of the PGF cross section is automatically generated by the evolution of the charm distribution. To avoid double counting we must therefore subtract from the coefficient function given by PGF the contribution which is generated by evolution in this way. As a consequence, above the charm threshold a smaller and smaller fraction of F_2^c will come from the direct photon-gluon fusion mechanism, and instead the main part will be generated by conventional parton evolution. In section 4 we use the new formulation to perform a NLO global analysis of deep inelastic and related hard scattering data. We find an excellent overall description with, in particular, a significant charm component of F_2 in the HERA regime. The analysis allows us to predict universal charm and bottom quark distributions, $c(x, Q^2)$ and $b(x, Q^2)$. In section 5 we present the partonic decomposition of F_2^c as a function of Q^2 and, for completeness, compare the PGF model estimates. We also give predictions for F_2^b . In section 6 we study the charm component of the longitudinal structure function F_L . Finally, in section 7, we give our conclusions.

2. The effects of the charm mass on evolution

As mentioned above, our aim is to develop the appropriate formalism to describe deep inelastic scattering which incorporates the production of a heavy quark pair (which for definiteness we take to be $c\bar{c}$) and which allows a universal charm parton distribution to be obtained from an analysis of these and other data. We can identify the charm mass effects in the structure functions $F_{2,L}^c$ which describe such scattering from the following subset of integrations³

$$\cdots \int \frac{dk_{T_{i-1}}^2}{k_{T_{i-1}}^2} \int \frac{dk_{T_i}^2 k_{T_i}^2}{(k_{T_i}^2 + m_c^2)^2} \int \frac{dk_{T_{i+1}}^2}{k_{T_{i+1}}^2} \cdots \quad (6)$$

where k_{T_i} are the transverse momenta of the t channel partons. The mass of the charm quark enters in the $k_{T_i}^2$ integration which results from the $g \rightarrow c\bar{c}$ transition, see Fig. 1. For the example of the parton chain shown in Fig. 1 it appears that m_c^2 should also have been retained in the integration over $k_{T_{i+1}}^2$. However, we show below that this is only needed at next-to-next-to-leading order (NNLO) in α_S .

³The general structure of the integrands is $k_T^2/(\text{propagator})^2$, which for massless partons $\sim 1/k_T^2$. The k_T^2 in the numerator arises from the spin structure of the parton vertex.

First we recall the kinematic regime responsible for the leading-order (LO) result. LO evolution corresponds to the resummation of the leading logarithm terms, $(\alpha_S \ln Q^2)^n$, which arise when the n emitted partons have strongly ordered transverse momenta ($\dots \ll k_{T_{i-1}}^2 \ll k_{T_i}^2 \ll k_{T_{i+1}}^2 \dots$). If two of the partons were to have comparable transverse momenta, $k_{T_j} \sim k_{T_{j+1}}$, then we would lose a $\ln Q^2$ and obtain instead a NLO contribution of the form $\alpha_S(\alpha_S \ln Q^2)^{n-1}$. We may write the Altarelli-Parisi splitting functions

$$P_{ji} = P_{ji}^{(0)} + \alpha_S P_{ji}^{(1)} + \dots \quad (7)$$

where $P^{(0)}$ is the LO form and $P^{(1)}$ gives the NLO correction. $P^{(1)}$ includes virtual corrections to the vertex and propagators as well as the possibility of producing a second ‘s channel’ parton with comparable transverse momentum.

2.1. LO evolution with charm

On the scale of the Altarelli-Parisi evolution in $\ln Q^2$, we see that to a good approximation

$$\frac{1}{1 + m_c^2/k_{T_i}^2} \approx \theta(k_{T_i}^2 - m_c^2), \quad (8)$$

that is the presence of the charm mass simply cuts out the contribution from the region $k_{T_i}^2 \lesssim m_c^2$. Indeed we will find, at LO accuracy, that we have massless three flavour evolution for $Q^2 < m_c^2$ and massless four flavour evolution for $Q^2 > m_c^2$; that is due to strong ordering ($k_{T_{i+1}}^2 \gg k_{T_i}^2$) we can neglect the charm mass in the $k_{T_{i+1}}^2$ integration of Fig. 1. Therefore at LO the singlet evolution equations have the symbolic form

$$\begin{aligned} \dot{g} &= P_{gg} \otimes g + \sum_q P_{gq} \otimes q + P_{gc} \otimes c \\ \dot{q} &= P_{qg} \otimes g + P_{qq} \otimes q \\ \dot{c} &= P_{cg} \otimes g + P_{cc} \otimes c \end{aligned} \quad (9)$$

where $q = u, d, s$ denotes the light quark density functions and c the charm density. We have abbreviated $P^{(0)}$ by P and $\dot{f} = (2\pi/\alpha_S)\partial f/\partial \ln Q^2$. At LO the quark mass effects are simply encapsulated by

$$P_{ci} = P_{ci}(m_c = 0) \theta(Q^2 - m_c^2) \quad (10)$$

with $i = g$ or c , and similarly for P_{gc} . Also the virtual contribution to P_{gg} must be modified

$$P_{gg} = \dots - \frac{1}{3} n_f \delta(1 - z) \quad (11)$$

with $n_f = 3 + \theta(Q^2 - m_c^2)$, and, of course, we must allow for the increase in the number of active flavours n_f in the running of α_S .

Although we show in (9) only the equation for \dot{c} , we note that each heavy quark (c, b, \dots) requires a separate singlet evolution equation [15] since their splitting functions have different

θ function contributions.

2.2. NLO evolution incorporating the charm mass

At NLO the inclusion of quark mass effects is a bit more complicated, although it turns out that we only have to take m_c into account in P_{cg} and then only in the LO part $P_{cg}^{(0)}$. (Of course as a consequence we must adjust the virtual corrections to P_{gg}). The argument is as follows.

We have to improve on approximation (8) of the k_{Ti}^2 integration in (6). To do this we divide the integral into two parts

$$\int \frac{dk_{Ti}^2 k_{Ti}^2}{(k_{Ti}^2 + m_c^2)^2} = \int \frac{d(k_{Ti}^2 + m_c^2)}{(k_{Ti}^2 + m_c^2)} - \int \frac{m_c^2 dk_{Ti}^2}{(k_{Ti}^2 + m_c^2)^2} \quad (12)$$

where the first term gives the leading logarithm contribution that we discussed in section 2.1. To be specific we have

$$\int_{k_{Ti-1}^2}^{Q^2} \frac{d(k_{Ti}^2 + m_c^2)}{(k_{Ti}^2 + m_c^2)} = \ln \frac{Q^2}{m_c^2} \quad (13)$$

for $k_{Ti-1}^2 \ll m_c^2$, which is equivalent to the threshold factor $\theta(k_{Ti}^2 - m_c^2)$ of (8). The second term in (12), which is concentrated in the region $k_{Ti}^2 \sim m_c^2$, gives a constant contribution. That is, it is a NLO contribution (containing a factor α_S without an accompanying $\ln Q^2$). It means that the m_c^2 effects need only be evaluated in the LO (one-loop) part of the $g \rightarrow c\bar{c}$ splitting function, $P_{cg}^{(0)}$. For instance consider the integration over k_{Ti+1} of Fig. 1 and the possibility of m_c^2 effects in P_{cc} . Clearly if $k_{Ti+1}^2 \gg m_c^2$ then the mass terms m_c^2/k_{Ti+1}^2 can be neglected. If, on the other hand, $k_{Ti+1}^2 \sim m_c^2$ then either $k_{Ti}^2 \ll m_c^2$ and $c(x, k_{Ti}^2) = 0$ or $k_{Ti}^2 \sim m_c^2$ and we lose two $\ln Q^2$ factors so that the contribution is NNLO, which we omit here. That is, at NLO there are no m_c effects in P_{cc} . A similar argument shows that this is also true for P_{gc} .

In summary, we have shown that at NLO P_{cc} and P_{gc} remain as in section 2.1, whereas

$$P_{cg} = P_{cg}^{(0)}(m_c) + \alpha_S P_{cg}^{(1)}(m_c = 0) \theta(Q^2 - m_c^2). \quad (14)$$

That is we need only evaluate the effect of the charm mass on the LO part of P_{cg} . As a consequence of the change in P_{cg} , we have to adjust the virtual correction to P_{gg} by an amount

$$\Delta P_{gg}^{(0)} = -\delta(1-z) \int_0^1 dz z \left(P_{cg}^{(0)}(z, m_c) - P_{cg}^{(0)}(z, m_c = 0) \right), \quad (15)$$

see section 2.3. This adjustment also restores energy-momentum conservation.

We note that instead of a charm density based on the Renormalization Group (RG) equations and leading-twist contributions⁴ we have introduced an arguably more physical parton density based on the leading $\ln Q^2$ decomposition of the Feynman diagrams retaining full mass

⁴The charm density in the conventional RG approach has been discussed recently in ref. [13], where the (leading twist) coefficients have been fully calculated at NNLO in the limit $Q^2 \gg m_c^2$.

effects. This charm density is universal⁵ and the partonic momentum sum rule is satisfied. Our definition of the parton density coincides⁶ with the conventional (massless) RG-based definition for $Q^2 \gg m_c^2$.

We have seen that in our approach at NLO we need only consider $m_c \neq 0$ effects in the LO diagrams. It is straightforward to extend the formalism to allow for charm mass effects in NNLO evolution. We need only consider $m_c \neq 0$ effects in the NLO diagrams. That is we need to evaluate the “blocks” $gg \rightarrow gg$, $gg \rightarrow c\bar{c}$, $q\bar{q} \rightarrow c\bar{c}$ to $\mathcal{O}(\alpha_S^2)$ with m_c^2 included explicitly, but only in the region $k_{Ti}^2 \sim m_c^2$. For example, for $gg \rightarrow gg$ we would need to evaluate the diagrams shown in Fig. 2.

2.3. Evaluation of quark mass effects in P_{cg}

We note that heavy quark mass effects were studied in refs. [15, 16] in terms of the anomalous dimensions of the moments of structure functions. However, it is difficult to apply the results to parton evolution, since in these early studies the mass correction plays the role of a higher twist contribution. As a consequence it violates the sum rules which reflect energy-momentum and baryon number conservation.

To restore the partonic picture we use “old fashioned” perturbation theory. That is we calculate the $g \rightarrow c\bar{c}$ splitting function P_{cg} in the infinite momentum frame with all three partons on-mass-shell. The parton four momenta are shown in Fig. 3. If the momentum of the gluon is large, $p_g \gg k_T$ and m_c , then the quark momentum is given by

$$k = \left(zp_g + \frac{m_c^2 + k_T^2}{2zp_g}; \quad \mathbf{k}_T, zp_g \right), \quad (16)$$

and similarly for k' with $z \rightarrow 1 - z$ and $\mathbf{k}_T \rightarrow -\mathbf{k}_T$. We may write the probability of the $g \rightarrow c\bar{c}$ splitting in the form

$$dw_{cg} = 8g^2 T_R \frac{d^2 k_T dk_{\parallel}}{(2\pi)^3} \left[\frac{1}{(2zp_g)^2 2(1-z)p_g} \right] \frac{\text{Sp}}{(\Delta E)^2} \quad (17)$$

with colour factor $T_R = \frac{1}{2}$ and where the $[\dots]$ contain the normalization factors of the two t channel and one s channel quark lines shown in Fig. 3. The energy denominators

$$\Delta E = E_{c\bar{c}} - E_g = \frac{m_c^2 + k_T^2}{2z(1-z)p_g} \quad (18)$$

⁵Of course, to use the parton density for other processes we must calculate the coefficient functions within the same framework.

⁶In the $Q^2 \gg m_c^2$ domain the evolution in Q^2 is exactly the same for both definitions, however the initial conditions of such an evolution, if it were to originate in the threshold region, would be different; compare our approach with that of ref. [13].

play the role of the quark propagators and the numerator

$$\begin{aligned} \text{Sp} &= \frac{1}{2} \delta_{ab}^\perp \text{Tr} \left(\gamma_a \frac{\not{k} + m_c}{2} \gamma_b \frac{-\not{k}' + m_c}{2} \right) \\ &= (m_c^2 + k_T^2) \frac{z^2 + (1-z)^2}{2z(1-z)} + m_c^2, \end{aligned} \quad (19)$$

where $\frac{1}{2}\delta_{ab}^\perp$ is the average over the two transverse polarizations of the (on mass shell) gluon and $\frac{1}{2}(\not{k} + m_c)$ is the quark density matrix. The factor of 8 in (17) arises from the sum over two polarizations of both the c and \bar{c} and allows for the t channel parton to be either c or \bar{c} .

To identify the splitting function we must rewrite (17) in the form

$$dw_{cg} = \frac{\alpha_S}{2\pi} \frac{dz}{z} \frac{dQ^2}{Q^2} P_{cg}^{(0)}(z, m_c, Q^2) \quad (20)$$

where $dk_\parallel = p_g dz$. The outstanding problem is therefore to determine the scale Q^2 appropriate for k_T^2 . The scale Q^2 should be chosen so that it correctly reproduces the timescale of the fluctuations of the gluon into the $c\bar{c}$ pair, that is

$$\Delta t \sim \frac{1}{\Delta E} = \frac{2E_g}{Q^2} \quad (21)$$

where ΔE is given by (18). It follows that the appropriate scale would be

$$Q^2 = 2p_g \Delta E = \frac{m_c^2 + k_T^2}{z(1-z)}. \quad (22)$$

Indeed this would be the physically natural scale to adopt. It represents the value of Q^2 ($\gtrsim 4m_c^2$) for which the resolution is sufficient to observe the individual c and \bar{c} partons within the short $g \leftrightarrow c\bar{c}$ fluctuation time Δt .

Unfortunately (22) is not the conventional scale used in the $\overline{\text{MS}}$ factorization scheme in the massless quark limit, or rather when $Q^2 \gg m_c^2$. To obtain parton densities which correspond to the $\overline{\text{MS}}$ scheme for $Q^2 \gg m_c^2$ we must take the evolution scale to be⁷

$$Q^2 = m_c^2 + k_T^2. \quad (23)$$

Of course we could use (22) as the evolution scale but then we would have to change the NLO splitting and coefficient functions. Since the NLO coefficient functions, not only for deep inelastic scattering but also for other processes, have been calculated in the $\overline{\text{MS}}$ scheme, it is clearly desirable to remain in this scheme. We therefore adopt (23) as the evolution scale. Then

⁷It is connected with the fact that in dimensional regularization in the $\overline{\text{MS}}$ scheme a factor $(k_T^2/\mu^2)^\epsilon$ is introduced into the dk_T^2/k_T^2 integration, see for example ref. [17]. Just as the $\overline{\text{MS}}$ and MS scheme coefficient functions differ simply by a constant factor, the coefficient functions in the $\overline{\text{MS}}$ scheme and the ‘natural’ scheme based on (22) differ by a factor which is a function of z .

we can use the $\overline{\text{MS}}$ NLO splitting functions $P^{(1)}$ for the massless quarks and gluons and for the massive quarks for $Q^2 \gg m_c^2$. Moreover for $Q^2 \gg m_c^2$ all the NLO coefficient functions have the $\overline{\text{MS}}$ form, except for one contribution which we discuss in section 3.2.

Now using the evolution scale (23) we have

$$P_{cg}^{(0)} = 2T_R \left[(z^2 + (1-z)^2) + \frac{2m_c^2}{Q^2} z(1-z) \right] \theta(Q^2 - m_c^2). \quad (24)$$

Recall that here P_{cg} stands for the splitting into both $c(\bar{c})$ and $\bar{c}(c)$. An analogous result for QED may be found in ref. [18]. The θ function represents the threshold ($k_T^2 = 0$) for generating in the evolution c and \bar{c} parton densities, which smoothly tend to the conventional $\overline{\text{MS}}$ distributions at high Q^2 . We see that even if at small x we have more than enough energy W to create a $c\bar{c}$ pair, $W^2 \simeq Q^2/x \gg 4m_c^2$, then it is possible that the value of Q^2 will be insufficient to resolve the c and \bar{c} pair within the short $g \leftrightarrow c\bar{c}$ fluctuation time Δt , that is when $Q^2 < 4m_c^2$.

The complete effect of the quark mass in the NLO splitting functions which involve the charm quark is contained in (24). It leads to the following correction to P_{gg}

$$\Delta P_{gg}^{(0)} = -\frac{2}{3} T_R \delta(1-z) \frac{m_c^2}{2Q^2} \theta(Q^2 - m_c^2), \quad (25)$$

see (15).

3. Coefficient functions for deep inelastic charm production

Just as for light quarks, the contribution of charm to the deep inelastic structure function F_2 is obtained from a convolution of the parton distributions and the coefficient functions. We have

$$F_2^c(x, Q^2) = \frac{8}{9} \int_x^1 dz \frac{x}{z} \left[C_{q=c}(z, Q^2, \mu^2) c\left(\frac{x}{z}, \mu^2\right) + C_g(z, Q^2, \mu^2) g\left(\frac{x}{z}, \mu^2\right) \right] \quad (26)$$

where, due to the quark mass, the coefficient functions have an explicit dependence on Q^2 . The charm quark coefficient function in (26) has the form

$$C_c = C_c^{(0)} + \frac{\alpha_S}{4\pi} C_c^{(1)} + \dots, \quad (27)$$

while for the gluon we have

$$C_g = \frac{\alpha_S}{4\pi} C_g^{(1)} + \dots \quad (28)$$

At NLO accuracy, to which we are working, we need only the coefficient functions that are shown explicitly in (27) and (28).

We see that at low scales below partonic threshold, $Q^2 < m_c^2$, where $c(x, Q^2) = 0$, the structure function F_2^c is described entirely by γg fusion, that is by the $C_g \otimes g$ convolution. However, we will find that as Q^2 increases from the charm threshold the contribution from the

γc interaction, $C_c \otimes c$, increases rapidly and soon becomes dominant. Of course, as we have already mentioned in the introduction, when the number of active flavours increases from 3 to 4 (as we pass through the threshold region) we must take care to avoid double counting. For example, if we were to take the limit in which charm is regarded as a heavy quark, and never a parton, then the entire contribution to F_2 is

$$F_2^c = \frac{\alpha_S}{4\pi} C_g^{\text{PGF}} \otimes g. \quad (29)$$

We call this fixed (three) flavour approach the photon-gluon fusion (PGF) approximation. From the above discussion it might appear that the PGF approximation, which clearly gives the correct NLO answer for $Q^2 < m_c^2$, will dramatically undershoot the true prediction as Q^2 increases above the charm resolution threshold. This is not so, since *part* of the Feynman diagram which is responsible for the important $C_c \otimes c$ parton evolution contribution is contained in $C_g^{\text{PGF}} \otimes g$ in the PGF approximation [14]. Thus to avoid double counting we will have to subtract this contribution from $C_g^{\text{PGF}} \otimes g$. The consistent treatment of charm mass effects will therefore allow us to quantify the accuracy of the PGF approximation to F_2^c as a function Q^2 .

3.1. The charm quark coefficient function for F_2^c

We must specify the coefficient functions for F_2^c that we introduced in (26)-(28). First the LO charm quark coefficient is given by

$$C_c^{(0)}(z, Q^2) = z \delta\left(z - 1/(1 + m_c^2/Q^2)\right) \left(1 + \frac{4m_c^2}{Q^2}\right) \quad (30)$$

where here z is defined with respect to the charm quark

$$z = z_0 = \frac{x}{x'} = \left(1 + \frac{m_c^2}{Q^2}\right)^{-1}. \quad (31)$$

The last equality follows directly from the mass-shell condition $(x'p + q)^2 = m_c^2$ where x' is the fraction of the momentum of the proton that is carried by the struck charm quark, see Fig. 4. The final factor in (30) allows for the F_L component of $F_2 = F_T + F_L$ where

$$\sigma_L/\sigma_T = 4m_c^2/Q^2. \quad (32)$$

Inserting $C_c^{(0)}$ of (30) into (26) gives a contribution to $F_2^c(x, Q^2)$ proportional to $xc(x', Q^2)$ where here the true scale is $\mu^2 = Q^2$. In fact at NLO all the $m_c \neq 0$ effects in the charm quark coefficient function occur in $C_c^{(0)}$. Indeed we justify in section 3.3 that at NLO we may simply use the massless quark expression for the coefficient $C_c^{(1)}$.

3.2. The gluon coefficient function for F_2^c

We may write the gluon coefficient function, defined in (28), in the form

$$C_g^{(1)} = C_g^{\text{PGF}} - \Delta C_g \quad (33)$$

where the PGF expression for F_2 is [19]

$$C_g^{\text{PGF}}(z, Q^2) = \left\{ \left[z^2 + (1-z)^2 + \frac{4m_c^2}{Q^2} z(1-3z) - \frac{8m_c^4}{Q^4} z^2 \right] \ln \frac{1+\beta}{1-\beta} + \left[8z(1-z) - 1 - \frac{4m_c^2}{Q^2} z(1-z) \right] \beta \right\} \theta \left(Q^2 \left(\frac{1}{z} - 1 \right) - 4m_c^2 \right). \quad (34)$$

β is the velocity of one of the charm quarks in the photon-gluon centre-of-mass frame

$$\beta^2 = 1 - \frac{4m_c^2 z}{Q^2(1-z)}. \quad (35)$$

The θ function in (34), $\theta(W^2 - 4m_c^2)$, represents the $c\bar{c}$ production threshold, where W is the c.m. energy. Its presence guarantees $\beta^2 \geq 0$. The ΔC_g term in (33) is necessary to avoid the double counting of the graph that we have already used to compute $P_{cg}^{(0)}$, see section 2.3. That is we must subtract from C^{PGF} the term $P_{cg}^{(0)} \otimes C_c^{(0)}$ that we already include in the parton evolution up to Q^2 . The z variable in the gluon coefficient functions is defined with respect to the gluon momentum fraction x_g ,

$$z = \frac{x}{x_g} = z_0 z' \quad (36)$$

where $z' = x'/x_g$, see Fig. 4. Thus the explicit form of the subtraction term is

$$\begin{aligned} \Delta C_g(z, Q^2) &= \int \frac{dz_0}{z_0} C_c^{(0)}(z_0, Q^2) \int_{Q_{\min}^2}^{Q^2} d \ln Q'^2 P_{cg}(z', Q'^2) \\ &= \left(1 + \frac{4m_c^2}{Q^2} \right) \int_{Q_{\min}^2}^{Q^2} d \ln Q'^2 P_{cg}(z', Q'^2). \end{aligned} \quad (37)$$

The lower limit of integration is given by the “partonic” θ function which is hidden in $P_{cg}(z', Q'^2)$, that is

$$Q_{\min}^2 = m_c^2. \quad (38)$$

The integration in (37) may be readily performed to give

$$\Delta C_g(z, Q^2) = \left[\{z'^2 + (1-z')^2\} \ln \left(\frac{Q^2}{m_c^2} \right) + z'(1-z') \left(2 - \frac{2m_c^2}{Q^2} \right) \right] \left(1 + \frac{4m_c^2}{Q^2} \right), \quad (39)$$

where we require $Q^2 > Q_{\min}^2$ and where $z' = z/z_0 = (1 + m_c^2/Q^2)z$.

It is interesting to consider the $m_c^2 \rightarrow 0$ limits of C_g^{PGF} and ΔC_g . We have

$$C_g^{\text{PGF}} \rightarrow \{z^2 + (1-z)^2\} \ln \left(\frac{1-z}{z} \frac{Q^2}{m_c^2} \right) + 8z(1-z) - 1 \quad (40)$$

as $m_c \rightarrow 0$, which differs from the exact $m_c = 0$ coefficient $C_g^{(1)}$ by the presence of Q^2/m_c^2 in the argument of the logarithm. However, from (39) we see that

$$\Delta C_g \rightarrow \{z^2 + (1-z)^2\} \ln \left(\frac{Q^2}{m_c^2} \right) + 2z(1-z) \quad (41)$$

as $m_c \rightarrow 0$, which removes the $\ln(Q^2/m_c^2)$ term in $C_g^{(1)} = C_g^{\text{PGF}} - \Delta C_g$.

The difference $C_g^{\text{PGF}} - \Delta C_g$ is exactly as in the conventional (massless) $\overline{\text{MS}}$ scheme apart from the final term $2z(1-z)$ in ΔC_g . This discrepancy is due to the different order in which the limits are taken in the calculation of the coefficient function. In the massless case we first take $m_q \rightarrow 0$ and then $\epsilon \rightarrow 0$, which is equivalent to taking the infrared cut-off $\Lambda > m_q$, whereas here we have first to take $\epsilon \rightarrow 0$ and then consider the $Q^2 \gg m_c^2$ limit. That is we can only neglect⁸ m_c^2 in $P_{cg}^{(0)}$ of (24) if $Q^2 \gg m_c^2$, whereas we need to evaluate P_{cg} in (37) down to $Q^2 = Q_{\min}^2 = m_c^2$.

3.3. Choice of scale

We now come to the choice of the scale μ^2 in (26). First we consider the convolution involving the gluon. The only dependence on the scale μ^2 in the coefficient function C_g is in the argument of α_S in (28). $C_g^{(1)}$ has no dependence on μ^2 since all the collinear singularities are regularized by the heavy quark mass provided that $\mu^2 \lesssim m_c^2$. Nevertheless we have to choose the scale μ^2 for α_S and the gluon distribution. Variation of the scale induces only NNLO contributions. There is as yet no complete calculation of the NNLO contributions⁹ (in our framework) applicable for all Q^2 which would introduce terms compensating the variation with scale. We must therefore attempt to identify the ‘natural’ scale for the process. We have already mentioned that the natural scale for the charm convolution is $\mu^2 = Q^2$.

Due to the different way that the scales enter, the $\alpha_S(\mu^2)\Delta C_g \otimes g(x/z, \mu^2)$ term does not exactly subtract the LO charm contribution which comes from the convolution $C_c^{(0)} \otimes c(x, Q^2)$. At first loop level the latter term is of the form

$$C_c^{(0)} \int_{m_c^2}^{Q^2} \frac{dq^2}{q^2} \alpha_S(q^2) P_{cg}^{(0)}(z) g\left(\frac{x}{z}, q^2\right). \quad (42)$$

Here we also take the natural choice¹⁰ of scale $\mu^2 = Q^2$ in the ΔC_g term. We see that over the whole range of integration in (42) we then have $q^2 < \mu^2$ and $\alpha_S(q^2) > \alpha_S(\mu^2)$. In other words the subtracted value of the ΔC_g term is a little less than needed, leading to a lack of smoothness in F_2^c near threshold. To diminish this effect we could reduce the scale μ^2 in the ΔC_g term by taking, say, $\mu^2 = \delta Q^2$ with $\delta < 1$. From the formal point of view the choice of μ^2 should not matter. In a NLO analysis it only induces changes at NNLO. However m_c^2 is not so large, and some of the deep inelastic data used in our fit will be at sufficiently low values of Q^2 that we sample scales $\mu^2 \gtrsim m_c^2$. In this Q^2 domain the analysis does have sensitivity to the choice of scale, showing the need for the NNLO formulation.

Now let us return to the charm quark coefficient function and, in particular, explain why the massless approximation is sufficient for $C_c^{(1)}$ at NLO. After the subtraction of the LO contribution (in an analogous way to (33) for the gluon coefficient function) the remaining coefficient

⁸If we were to neglect m_c^2 in (24) for all Q^2 then the additional $2z(1-z)$ contribution in ΔC_g would disappear.

⁹However for $Q^2 \gg m_c^2$ see [13].

¹⁰Of course we do not want $\mu^2 < m_c^2$ and so, in the analysis described in section 4, we take $\mu^2 = \max\{Q^2, m_c^2\}$.

$C_c^{(1)}$ contains no $\ln Q^2$ terms. Recall that in the presence of a heavy quark mass we lose a logarithm (see (12) and (13)). Therefore at NLO we need only consider $m_c \neq 0$ in the LO diagrams. Similarly at NNLO we only require $m_c \neq 0$ in the NLO graphs and so on. Therefore the (non-logarithmic $\mathcal{O}(\alpha_S)$) contribution $C_c^{(1)}$ is only needed when $Q^2 \gg m_c^2$, as was discussed in section 2.2 after Eq. (13). For $Q^2 \lesssim m_c^2$ the charm density $c(x, Q^2) = 0$, while for $Q^2 \gtrsim m_c^2$ two powers of $\ln Q^2$ are lost (one in P_{cg} and one in $C_c^{(1)}$) and so this region contributes only at NNLO. Thus we can set $m_c = 0$ in $C_c^{(1)}$. Of course we must use the same definition of the scale Q^2 , (23), as for massless evolution in the $\overline{\text{MS}}$ scheme.

3.4. The resolution of charm

Although we now have a definite framework which enables us to incorporate a $m_c \neq 0$ charm parton into a parton analysis, we immediately encounter a problem when we confront the data. The charm density rises rapidly as we evolve up from the threshold $Q^2 = m_c^2$ (required by the $\overline{\text{MS}}$ scale (23)) such that in the region $Q^2 \gtrsim m_c^2$ it is in conflict with the data. The reason is clear. The physically reasonable scale at which the charm parton may be resolved is given by (22) with a threshold at $Q^2 = 4m_c^2$. In order to implement this behaviour we introduce a factor

$$f = \left(1 - \frac{4m_c^2}{Q^2}\right) \theta\left(1 - \frac{4m_c^2}{Q^2}\right) \quad (43)$$

into the charm coefficient function C_c of (27) and (30) which, via (37), then feeds through into ΔC_g .

At first sight the introduction of the ‘ad hoc’ factor of f appears to modify even the LO result, which in symbolic form now may be written

$$F_2^c(\text{LO}) = f C_c^{(0)} \otimes c. \quad (44)$$

This is not so. In fact we will see that the modifications due to the introduction of f only enter at NNLO. At LO we have strong ordering in transverse momenta. LO contributions therefore only occur for $Q^2 \gg m_c^2$, where $f \rightarrow 1$. This reflects the fact that mass effects correspond to the loss of a factor of $\ln Q^2$ and only contribute at the next order of α_S . So the NLO contribution is changed, but only by an amount $\sim \alpha_S \ln(4m_c^2/m_c^2) \sim \text{const.} \alpha_S$ coming from evolution over the limited interval $m_c^2 < Q^2 \sim 4m_c^2$. However even this contribution is cancelled by the ΔC_g coefficient function. To see this we inspect the NLO form

$$F_2^c(\text{LO} + \text{NLO}) = f \left(C_c^{(0)} + \alpha_S C_c^{(1)} \right) \otimes c + \alpha_S C_g^{(1)} \otimes g. \quad (45)$$

To obtain the gluon coefficient function $C_g^{(1)}$, recall that we evaluated $\gamma g \rightarrow c\bar{c}$ at $\mathcal{O}(\alpha_S)$, which we denoted by $\alpha_S C_g^{\text{PGF}}$, and then subtracted the LO part ($\sim \alpha_S \ln Q^2$), which was already included,

$$\begin{aligned} F_2^c(\text{LO}) &= f C_c^{(0)} \otimes c \\ &= f C_c^{(0)} \otimes \alpha_S \ln Q^2 P_{cg}^{(0)} \otimes g \equiv \alpha_S \Delta C_g^{(1)} \otimes g, \end{aligned} \quad (46)$$

where it is sufficient to use the LO expression for the charm density. Thus

$$\begin{aligned}\alpha_S C_g^{(1)} &= \alpha_S \left(C_g^{\text{PGF}} - \Delta C_g^{(1)} \right) \\ &= \alpha_S C_g^{\text{PGF}} - f C_c^{(0)} \otimes \alpha_S \ln Q^2 P_{cg}^{(0)} .\end{aligned}\tag{47}$$

The last term of (47) exactly cancels the first term of (45), so

$$F_2^c(\text{LO} + \text{NLO}) = \alpha_S C_g^{\text{PGF}} \otimes g + f \alpha_S C_c^{(1)} \otimes c .\tag{48}$$

Thus the introduction of the ad hoc factor f gives rise to a modification $(1 - f)\alpha_S C_c^{(1)} \otimes c$ which only enters at NNLO. Indeed, in the appendix we show precisely how the modification is cancelled when working to NNLO.

Thus, in summary, in the NLO global parton analysis of section 4 we make the replacement

$$C_c^{(0)} \rightarrow f C_c^{(0)}\tag{49}$$

in (30), and similarly for $C_c^{(1)}$. Hence (39) becomes

$$\Delta C_g \rightarrow f \Delta C_g ,\tag{50}$$

where f is given by (43). After the introduction of the factor f , only the PGF contribution survives in the region $Q^2 < 4m_c^2$ below the resolution threshold, even though we have a non-zero charm parton density for $Q^2 > m_c^2$. As we evolve above the resolution threshold $Q^2 = 4m_c^2$ the charm parton component of F_2^c rapidly becomes important.

4. Charm as a parton in a global analysis

The measurements of F_2 at HERA have become much more precise with errors as small as $\pm 3\%$ or less. Moreover, since the charm component F_2^c of F_2 is about 0.25 in the HERA regime it is important to improve the treatment of charm in the analysis of deep inelastic scattering data. This was the objective of sections 2 and 3 above. The new formalism incorporates the heavy quark masses in the parton evolution equations and allows a determination of the (universal) charm and bottom quark densities. Indeed we can predict $c(x, Q^2)$ and $b(x, Q^2)$, as well as the charm and bottom components of F_2 , directly from a knowledge of the gluon and other quark densities. There are no free parameters, although the results do depend on the values of m_c and m_b , and, as usual, on the truncation of the perturbation expansion. As in previous analyses, we work to NLO.

The new framework is a significant advance on the existing treatment of charm in deep inelastic scattering. Recall that two different types of approach are used at present. In the first, charm is set to zero below some scale ($c(x, Q^2) = 0$ for $Q^2 < \mu^2$) and for $Q^2 > \mu^2$ the charm distribution is evolved assuming that $m_c = 0$. Although this procedure is clearly inaccurate in the $c\bar{c}$ threshold region, the parameter μ is chosen so that the fixed-target F_2^c data are well described. Secondly, we have the PGF approach [10, 11] based on the calculation of $\gamma^* g \rightarrow c\bar{c}$

with the correct kinematics, but in which c is not treated as a parton. As we have seen, this gives the correct description of F_2^c for $Q^2 < m_c^2$ and should remain a reasonable approximation to F_2^c for $Q^2 \gtrsim m_c^2$. However, the PGF model will inevitably break down at larger Q^2 values when charm can no longer be treated as a non-partonic heavy object and when it begins to evolve more like the lighter components of the quark sea.

Actually there exists in the literature a third, hybrid, approach [14]. Charm is treated as a new massless parton above $Q^2 = m_c^2$. That is the m_c^2 effects are neglected in the splitting functions, although they are included in the coefficient functions to NLO. This is not quite correct since the neglected m_c^2 effects would give NLO contributions during the evolution.

Before we present our predictions for $c(x, Q^2)$ and $b(x, Q^2)$, we perform a NLO global analysis of deep inelastic and related data which incorporates the $m_q \neq 0$ parton evolution procedure that we introduced in sections 2 and 3. This may be regarded as a small refinement of the global analysis determination of the gluon and light quark densities of ref. [8], but it does allow the gluon (and other parton) distributions to readjust themselves to accommodate the new treatment of $c(x, Q^2)$. Recall that the heavy quark distributions, $c(x, Q^2)$ and $b(x, Q^2)$, do not contain any free parameters apart, of course, from m_c and m_b . Motivated by QCD sum rules, we take $m_c = 1.35$ GeV and $m_b = 4.3$ GeV [20]. We show the effects of varying the value of m_c when we discuss the description of F_2^c . In fact we find that the overall description of the data (and in particular of F_2 in the HERA regime) improves compared to our previous analyses [8]. The only change to the data set that we use is the addition of the final NMC data [21] for F_2 .

We shall present full details of the new global analysis ¹¹ in a future paper in which we will discuss the improvements of the deep inelastic data and their implications. However, in Table 1 we illustrate the quality of the new fit relative to our previous fit that best described the HERA data, MRS(R2) [8]. We see that despite now having a prescribed charm distribution, the quality of the new fit is comparable to or actually slightly better (particularly for the small- x F_2 measurements) than that of the previous analysis.

The HERA data lie in the region where F_2^c/F_2 is largest and there is clear improvement in the new fit for these data. The value of α_S resulting from the new fit is $\alpha_S(M_Z^2) = 0.118$, intermediate to the values 0.113 and 0.120 of MRS(R1) and (R2) and the lower χ^2 for the BCDMS data in the Table is due to this. Our prescription for $\alpha_S(Q^2)$ across charm and bottom thresholds is to match the values at $Q^2 = m_c^2$, and again at $Q^2 = m_b^2$. Thus we define

$$\alpha_{S(4)}(Q^2) = \alpha_S(Q^2, 4) \quad (51)$$

and take, for 5 flavours,

$$\alpha_{S(5)}^{-1}(Q^2) = \alpha_S^{-1}(Q^2, 5) + \alpha_S^{-1}(m_b^2, 4) - \alpha_S^{-1}(m_b^2, 5), \quad (52)$$

¹¹The FORTRAN code for this set of partons, MRRS, together with the code for computing each flavour component to F_1 , F_2 and F_L is available by electronic mail from W.J.Stirling@durham.ac.uk, or directly from <http://durpdg.dur.ac.uk/HEPDATA/MRS>.

Experiment	# data	χ^2	
		MRRS	MRS(R ₂)
H1 F_2^{ep}	193	133	149
ZEUS F_2^{ep}	204	290	308
BCDMS $F_2^{\mu p}$	174	271	320
NMC $F_2^{\mu p}$	130	145	134
NMC $F_2^{\mu d}$	130	119	98
E665 $F_2^{\mu p}$	53	60	62
E665 $F_2^{\mu d}$	53	54	60
SLAC F_2^{ep}	70	96	95

Table 1: χ^2 values for some of the data [5, 6, 21, 22, 23, 24] used in the global fit. Note the larger χ^2 values for the E665 points [24] than those quoted in ref. [8] — these result from our correcting our previous incorrect treatment of the E665 experimental errors.

while for 3 flavours we have

$$\alpha_{S(3)}^{-1}(Q^2) = \alpha_S^{-1}(Q^2, 3) + \alpha_S^{-1}(m_c^2, 4) - \alpha_S^{-1}(m_c^2, 3). \quad (53)$$

In Fig. 5 we show the flavour decomposition of the sea as a function of Q^2 for two different values of x . Recall that there are now no input parameters for the heavy quark distributions, $c(x, Q^2)$ and $b(x, Q^2)$, and that they are determined in terms of the gluon (and other parton) distributions.

We show the description of both the fixed target and HERA data for F_2^c in the next section. The charm data are not used in the global fit. However, when they become more precise these data should be included as they will provide a significant extra constraint on the gluon distribution. The gluon density from the new fit compares very closely with that of MRS(R2). The new gluon is more ‘valence-like’ at $Q_0^2 = 1 \text{ GeV}^2$, but for $Q^2 \geq 2 \text{ GeV}^2$ both gluon distributions rise at small x and become increasingly similar as Q^2 continues to increase.

5. The structure of F_2^c

Fig. 6 shows the partonic decomposition of F_2^c as given by (26), which may be written in the symbolic form

$$F_2^c = C_c \otimes c + C_g \otimes g. \quad (54)$$

The gluonic component gives the total production below the charm resolution threshold, $Q^2 < 4m_c^2$. However, the component driven by the charm distribution rises rapidly above threshold and becomes dominant at larger Q^2 . We also show for comparison the photon-gluon fusion prediction $C^{\text{PGF}} \otimes g$. The PGF model and our prediction are identical below threshold, $Q^2 <$

$4m_c^2$. Above threshold we see that the rapid onset of the charm parton component $C_c \otimes c$ is largely balanced by the subtraction ΔC_g from the PGF result. Let us discuss in turn the behaviour of F_2^c near the charm threshold and then at large Q^2 .

The lack of smoothness of F_2^c apparent in Fig. 6 in the charm threshold region is due to the mismatch of the subtraction term $\alpha_S \Delta C_g \otimes g$ with $C_c^{(0)} \otimes c = C_c^{(0)} \otimes \alpha_S P_{cg}^{(0)} \otimes g$ with different scales of α_S and g in the two terms, see section 3.3. In the ΔC_g term the scale is μ^2 (where we have taken the natural choice $\mu^2 = Q^2$, or rather $\mu^2 = \max\{Q^2, m_c^2\}$), whereas α_S and g in the second term are evaluated at scales varying over the convolution interval m_c^2 to Q^2 . Of course we could have reduced the mismatch by choosing a smaller scale μ^2 , more representative of the m_c^2 to Q^2 integration interval. But formally in a NLO analysis the choice of scale μ^2 (and the mismatch) should not matter. It only gives contributions at NNLO. However in the charm threshold region $\alpha_S(\mu^2)$ is relatively large and we are sensitive to the choice of μ^2 . If the NNLO formalism were available the behaviour of $F_2^c(x, Q^2)$ in the charm threshold region would be more stable under variations of μ^2 , and would have a smoother form in Q^2 .

As expected these problems evaporate at larger values of Q^2 . Away from the charm threshold region ($Q^2 \gtrsim 20 \text{ GeV}^2$) the predictions for F_2^c for different μ^2 rapidly approach each other as Q^2 increases and become insensitive to the choice of scale μ^2 . The effects of the *evolution* of the charm density are evident. A measure of the effect is the difference between the prediction of F_2^c (continuous curves in Fig. 6) and that obtained in the PGF model (dot-dashed curves). By $Q^2 = 100 \text{ GeV}^2$, for example, for $x = 0.05$ (0.005) the improved description, in which charm is treated as a parton, lies some 75% (30%) above the PGF model.

The comparisons of the predictions for F_2^c with the EMC and the HERA data are shown in Fig. 7. The overall agreement over quite an extensive range of x and Q^2 is good. The dotted and dashed curves in Fig. 7 show the effect of taking $m_c = 1.2$ and 1.5 GeV respectively, rather than the central value, $m_c = 1.35 \text{ GeV}$, which we use throughout this paper.

Fig. 8 shows the fraction of charm deep inelastic events as a function of Q^2 for selected values of x . The strong production of charm at HERA is evident; moreover we see a sensitive dependence on x and Q^2 . If a significant fraction of the numerous charm events can be cleanly isolated in the experiments at HERA then the resulting precision measurement of F_2^c , coupled with the measurement of F_2 , will provide a powerful double constraint on the gluon distribution, as well as offering a stringent scheme independent test of QCD along the lines of that using F_2 and F_L proposed by Catani [25].

6. Predictions for F_L^c

We may also use the new formalism which incorporates the quark mass to calculate the charm component F_L^c of the longitudinal structure function. We use expressions that are identical to (26)–(28) and (33) but with the coefficient functions $C_{q=c}$ and C_g that are appropriate to F_L^c . For the quark coefficient we have

$$C_c^{(0)} = \frac{4m_c^2}{Q^2} z \delta \left(z - (1 + m_c^2/Q^2)^{-1} \right), \quad (55)$$

whereas for $C_c^{(1)}$ we may use the massless quark expression, since we are working to NLO accuracy. For the gluon coefficient for F_L^c we have

$$C_g^{(1)} = C_g^{\text{PGF}} - \Delta C_g \quad (56)$$

where

$$C_g^{\text{PGF}}(z, Q^2) = 4\beta z(1-z) - 8z^2 \frac{m_c^2}{Q^2} \ln \frac{1+\beta}{1-\beta} \quad (57)$$

with $Q^2 > 4m_c^2 z/(1-z)$, where the quark velocity β is given by (35). Here the subtraction term is

$$\Delta C_g(z, Q^2) = \frac{4m_c^2}{Q^2} \left[\dots \right] \quad (58)$$

where $[\dots]$ is the expression in the square brackets in (39). For ΔC_g to be non-zero we require $Q^2 > Q_{\text{min}}^2$, where Q_{min}^2 is given by (38). Just as for the coefficient functions for F_2 , we also include the factor f of (43) in $C_c^{(0,1)}$ and ΔC_g .

In Fig. 9 we present the predictions for F_L in terms of the ratio $R^c = F_L^c/F_T^c$. Due to the factor $4m_c^2/Q^2$ in the coefficient function of the LO charm component given in (55), we have a pronounced peak in R^c just above the resolution threshold, $Q^2 = 4m_c^2$. In this region R^c is sensitive to the precise choice of the scale μ^2 . As expected R^c decreases as Q^2 increases, as well as becoming more stable to changes of scale. The NLO gluonic component gives a smaller value of R^c than the charm component. Hence the peak is more pronounced at larger x when the gluonic component is less important. We also show in Fig. 9 the values of $R = F_L/F_T$.

7. Conclusions

We have determined the charm and bottom quark densities of the proton taking into account the effects of their non-zero mass. In particular we have presented a formalism which incorporates m_c and m_b into the Altarelli-Parisi splitting functions and in the coefficient functions in a consistent way. We can therefore evolve up in Q^2 taking proper account of the heavy quark thresholds. At NLO accuracy we show that the main effect of the quark mass is in the splitting function $P_{cg}^{(0)}$ (or $P_{bg}^{(0)}$).

We showed that the threshold for the charm density, $c(x, Q^2)$, occurs at $Q^2 = m_c^2$. On the other hand we know that the threshold for deep inelastic $c\bar{c}$ production is given by $W^2 = 4m_c^2$, or equivalently $Q^2 = 4m_c^2(1-x)/x$, which for small x occurs below the partonic threshold $Q^2 = m_c^2$. This apparent contradiction has a simple explanation. In the region $Q^2 < 4m_c^2$ we find that Q^2 is too small to allow sufficient time to observe the $g \rightarrow c\bar{c}$ fluctuations which occur within the proton. Here the photon-gluon fusion mechanism, $\gamma^* g \rightarrow c\bar{c}$, gives the complete answer. For evolution above the partonic resolution threshold the structure of F_2^c is more interesting. The charm component $\gamma^* c \rightarrow c$ with a spectator \bar{c} quark (or vice-versa with $c \leftrightarrow \bar{c}$) increases rapidly and soon exceeds the gluonic contribution $\gamma^* g \rightarrow c\bar{c}$ which only enters at NLO. In the partonic description the LO part of the gluon now has the structure $(g \rightarrow c\bar{c}) \otimes (\gamma^* c \rightarrow c)$.

To avoid double counting we must therefore subtract this LO contribution of the gluon and keep only the part coming from $C_g^{(1)}$.

In addition to its importance in determining the charm quark density $c(x, Q^2)$, the correct formulation of charm mass effects in evolution has become essential in order to obtain an accurate description of F_2 in the HERA domain. The reasons are that the charm component of F_2 is appreciable ($F_2^c/F_2 \sim 0.25$ for $x \sim 0.001$ and $Q^2 \sim 25 \text{ GeV}^2$) and that the measurements of F_2 at HERA are now much more precise.

In summary, in this paper we have shown how to treat charm as a parton for all values of Q^2 . The new NLO partonic formulation, which incorporates $m_c \neq 0$ effects, has the following important features.

- (i) The charm distribution contains no free parameters, except m_c .
- (ii) The partons are universal (that is they can be used in the NLO description of all hard scattering processes initiated by protons).
- (iii) the splitting and coefficient functions coincide with those of the (massless) $\overline{\text{MS}}$ scheme for $Q^2 \gg m_c^2$ (with the one exception discussed in section 3.2).
- (iv) The momentum and flavour sum rules are conserved.
- (v) There is a definite prescription to enable the formulation to be extended to include $m_c \neq 0$ effects at NNLO and higher orders.
- (vi) The new framework, in which the charm density is defined in terms of a leading $\ln Q^2$ decomposition of the Feynman diagrams retaining the full mass effects, is applicable in the important threshold¹² region $Q^2 \gtrsim m_c^2$.

Finally, we have used the new prescription to perform a global analysis of deep inelastic and related hard scattering data and generated charm and bottom quark densities. The analysis *predicts* the values of F_2^c (and F_2^b). We find that the predictions for F_2^c show some sensitivity to NNLO effects in the charm threshold region ($Q^2 \sim m_c^2$), but become increasingly stable as Q^2 increases above about 20 GeV^2 . We find good agreement with the EMC and H1 measurements of F_2^c . These data, which span a wide range of (x, Q^2) , were not used in the global analysis. Clearly as the experimental precision increases they should be included, and will impose a valuable additional constraint in the determination of the parton densities, and of the gluon in particular.

Acknowledgements

We thank Valery Khoze, Jan Kwiecinski, Jack Smith and Robert Thorne for useful discussions. MGR thanks the Royal Society for a Fellowship grant, and for support from the Russian Fund of Fundamental Research 96 02 17994.

¹²The latter region is inaccessible to the RG approach to the charm density. Indeed it is not clear how to formulate the RG approach when an extra dimensionful parameter (m_c) is essential. For $Q^2 \gg m_c^2$ our formulation reduces to the conventional RG massless parton approach.

Appendix

Here we demonstrate how, if we were to work at NNLO, the factor f of (43) contributes only at NNNLO. If, for simplicity, we neglect the light quarks, then we have in analogy to (45)

$$F_2^c(\dots + \text{NNLO}) = f \left(C_c^{(0)} + \alpha_S C_c^{(1)} + \alpha_S^2 C_c^{(2)} \right) \otimes c + \left(\alpha_S C_g^{(1)} + \alpha_S^2 C_g^{(2)} \right) \otimes g . \quad (\text{A1})$$

$C_g^{(2)}$ is given by the $\mathcal{O}(\alpha_S^2)$ expression for the photon-gluon cross section, $\alpha_S^2 C_g^{(2)\text{PGF}}$ minus the $\alpha_S^2 \ln^2 Q^2$ and $\alpha_S^2 \ln Q^2$ contributions which are already generated within the LO+NLO formalism. That is

$$\alpha_S^2 C_g^{(2)} = \alpha_S^2 C_g^{(2)\text{PGF}} - \Delta C_g^{(2)} \quad (\text{A2})$$

with

$$\begin{aligned} \Delta C_g^{(2)} = & f C_c^{(0)} \otimes \left[\left(\alpha_S \ln Q^2 \right)^2 \left(P_{cg}^{(0)} \otimes P_{gg}^{(0)} + P_{cc}^{(0)} \otimes P_{cg}^{(0)} \right) \otimes g + \alpha_S^2 \ln Q^2 P_{cg}^{(1)} \otimes g \right] \\ & + f \alpha_S C_c^{(1)} \otimes \alpha_S \ln Q^2 P_{cg}^{(0)} \otimes g + \alpha_S C_g^{(1)} \otimes \alpha_S \ln Q^2 P_{gg}^{(0)} \otimes g . \end{aligned} \quad (\text{A3})$$

Inserting (A2) into (A1) and cancelling terms, we find that the residual $\mathcal{O}(\alpha_S^2)$ part of F_2^c is

$$F_2^c(\text{NNLO}) = \alpha_S^2 C_g^{(2)\text{PGF}} \otimes g + f \alpha_S^2 C_c^{(2)} \otimes c , \quad (\text{A4})$$

in analogy to (48). The modification $(1 - f) \alpha_S^2 C_c^{(2)} \otimes c$ due to the introduction of the ad hoc factor f is now of NNNLO.

References

- [1] W.-K. Tung, Proc. of Int. Workshop on Deep Inelastic Scattering and Related Subjects (DIS 94), Eilat 1994, Ed. A. Levy (World Scientific, 1994), p.29.
- [2] H1 collaboration: C. Adloff *et al.*, DESY-96-138, July 1996.
- [3] ZEUS collaboration: “ D^* Production in Deep Inelastic Scattering at HERA”, contribution to the XXVIII Int. Conf. on HEP, Warsaw 1996.
- [4] EMC collaboration: J.J. Aubert *et al.*, Nucl. Phys. **B213** (1983) 31.
- [5] H1 collaboration: S. Aid *et al.*, Nucl. Phys. **B470** (1996) 3.
- [6] ZEUS collaboration: M. Derrick *et al.*, Zeit. Phys. **C69** (1996) 607; preprint DESY 96-076 (1996), to be published in Zeit. Phys.
- [7] A.D. Martin, R.G. Roberts and W.J. Stirling, Phys. Rev. **D50** (1994) 6734.
- [8] A.D. Martin, R.G. Roberts and W.J. Stirling, Phys. Lett. **B387** (1996) 419.
- [9] M. Glück, E. Hoffmann and E. Reya, Z. Phys. **C13** (1982) 119.
- [10] M. Glück, E. Reya and M. Stratmann, Nucl. Phys. **B422** (1994) 37.
- [11] A.J. Askew, J. Kwiecinski, A.D. Martin and P.J. Sutton, Phys. Rev. **D47** (1993) 3775; J. Kwiecinski, A.D. Martin and P.J. Sutton, Z. Phys. **C71** (1996) 585.
- [12] E. Laenen, S. Riemersma, J. Smith and W.L. van Neerven, Nucl. Phys. **B392** (1993) 162.
- [13] M. Buza, Y. Matiounine, J. Smith and W.L. van Neerven, preprint NIKHEF/96-027 (1996).
- [14] M.A.G. Aivazis, J.C. Collins, F.I. Olness and W.-K. Tung, Phys. Rev. **D50** (1994) 3102.
- [15] B.J. Edwards and T. Gottschalk, Nucl. Phys. **B196** (1982) 328; Yu. P. Ivanov, Sov. J. Nucl. Phys. **44** (1986) 317.
- [16] T. Gottschalk, Nucl. Phys. **B191** (1981) 227.
- [17] G. Curci, W. Furmanski and R. Petronzio, Nucl. Phys. **B175** (1980) 27.
- [18] V.A. Khoze *et al.*, Nucl. Phys. **B65** (1973) 381.
- [19] E. Witten, Nucl. Phys. **B104** (1976) 445; M.A. Shifman, A.I. Vainshtein and V.I. Zakharov, Nucl. Phys. **B136** (1978) 157; M. Glück and E. Reya, Phys. Lett. **B83** (1979) 98.

- [20] *Review of Particle Physics*, Particle Data Group, R.M. Barnett *et al.*, Phys. Rev. **D54** (1996) 1.
- [21] NM Collaboration: M. Arneodo *et al.*, Nucl. Phys. (in press), hep-ph-9610231.
- [22] BCDMS collaboration: A.C. Benvenuti *et al.*, Phys. Lett. **B223** (1989) 485.
- [23] L.W. Whitlow *et al.*, Phys. Lett. **B282** (1992) 475.
L.W. Whitlow, preprint SLAC-357 (1990).
- [24] E665 collaboration: M.R. Adams *et al.*, Phys. Rev. **D54** (1996) 3006.
- [25] S. Catani, to be published in Proc. of Workshop on Deep Inelastic Scattering and Related Phenomena (DIS 96), Rome, hep-ph/9608310.

Figure Captions

- Fig. 1 Part of the parton chain occurring in the description of deep inelastic scattering which contains the $g \rightarrow c\bar{c}$ transition.
- Fig. 2 An example of a “block” diagram along the parton chain, which gives NNLO charm mass effects if the two s channel charm quarks have comparable transverse momenta. Then the charm mass should be retained for all the quark lines that are shown.
- Fig. 3 The diagram used to calculate the charm mass effects in $P_{cg}^{(0)}$.
- Fig. 4 The variables used in the discussion of the coefficient functions $C_{q=c}(z, Q^2)$ and $C_g(z, Q^2)$. For the charm quark function the variable $z = x/x'$, while for the gluon function $z = x/x_g$, see eq. (31) and (36) respectively; x is the usual Bjorken $x \equiv Q^2/2p \cdot q$.
- Fig. 5 The flavour decomposition of the quark sea distribution of the proton as a function of Q^2 at two values of x . The total sea is given by $\mathcal{S} = 2(\bar{u} + \bar{d} + s + c + b)$.
- Fig. 6 The partonic decomposition of F_2^c as a function of Q^2 for $x = 0.05$ and $x = 0.005$. For $Q^2 \leq 4m_c^2$ there is only the contribution from $C_g = C_g^{PGF}$. For larger Q^2 , $C_g = C_g - \Delta C_g$ and the total F_2^c is the sum of this contribution and that from C_c .
- Fig. 7 The description of the EMC and HERA measurements of F_2^c . The solid line corresponds to our new fit with $m_c = 1.35$ GeV. The dashed and dotted lines correspond to taking $m_c = 1.5$ and 1.2 GeV respectively, with all other parameters unchanged.
- Fig. 8 The ratios F_2^c/F_2 and F_2^b/F_2 at fixed values of Q^2 resulting from the new global fit (in which we take $m_c = 1.35$ GeV and $m_b = 4.3$ GeV). The experimental data point shows the estimate from ref. [2] for F_2^c/F_2 in the HERA kinematic region, $10 \text{ GeV}^2 < Q^2 < 100 \text{ GeV}^2$.
- Fig. 9 The predictions for $R^c = F_L^c/F_T^c$ and $R = F_L/F_T$ as a function of Q^2 for $x = 0.0005$ and $x = 0.05$.

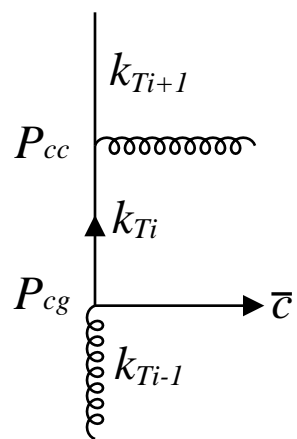


Fig.1

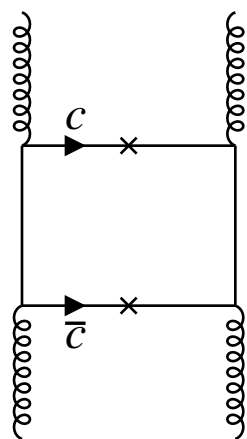


Fig.2

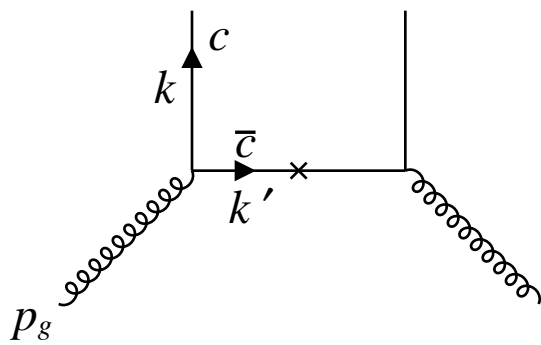


Fig.3

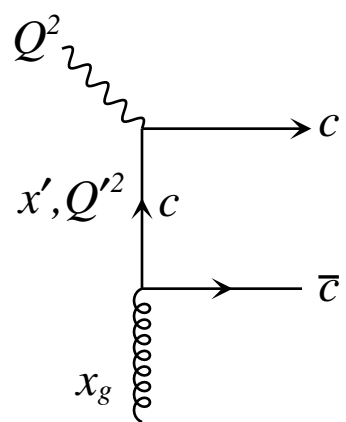


Fig.4

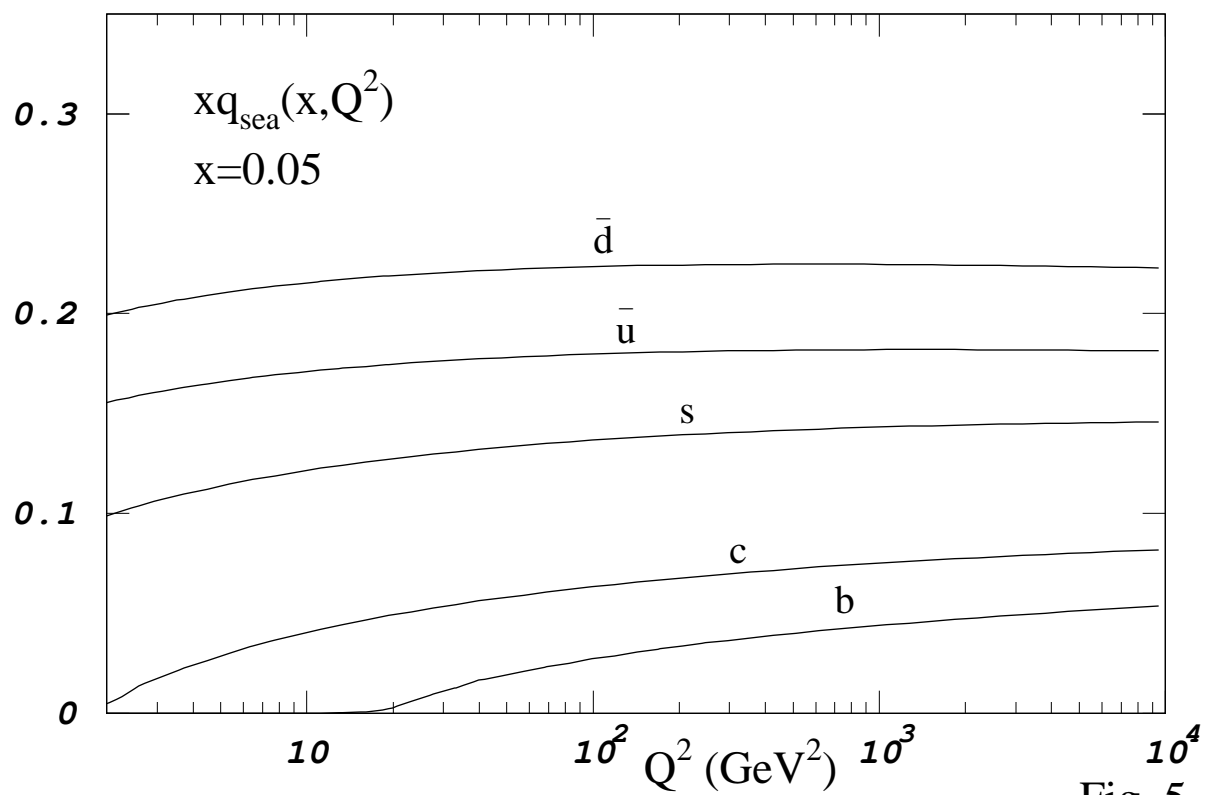
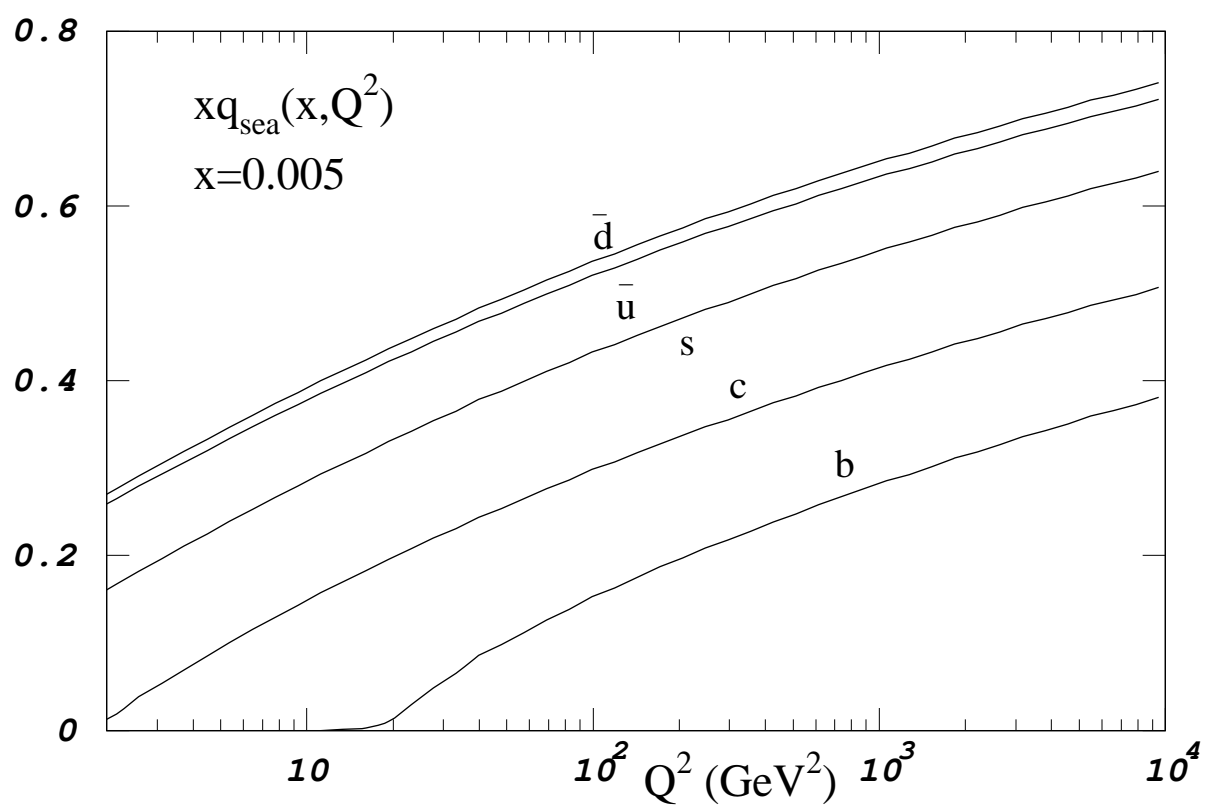


Fig. 5

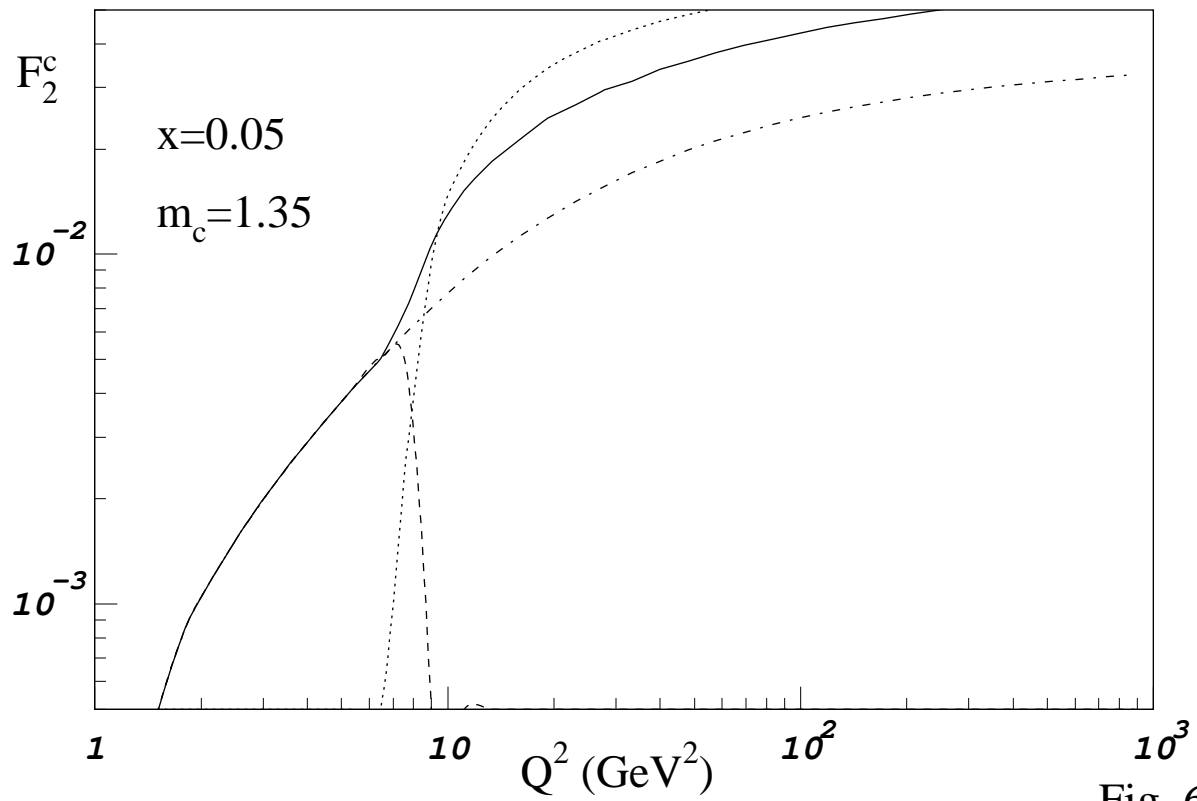
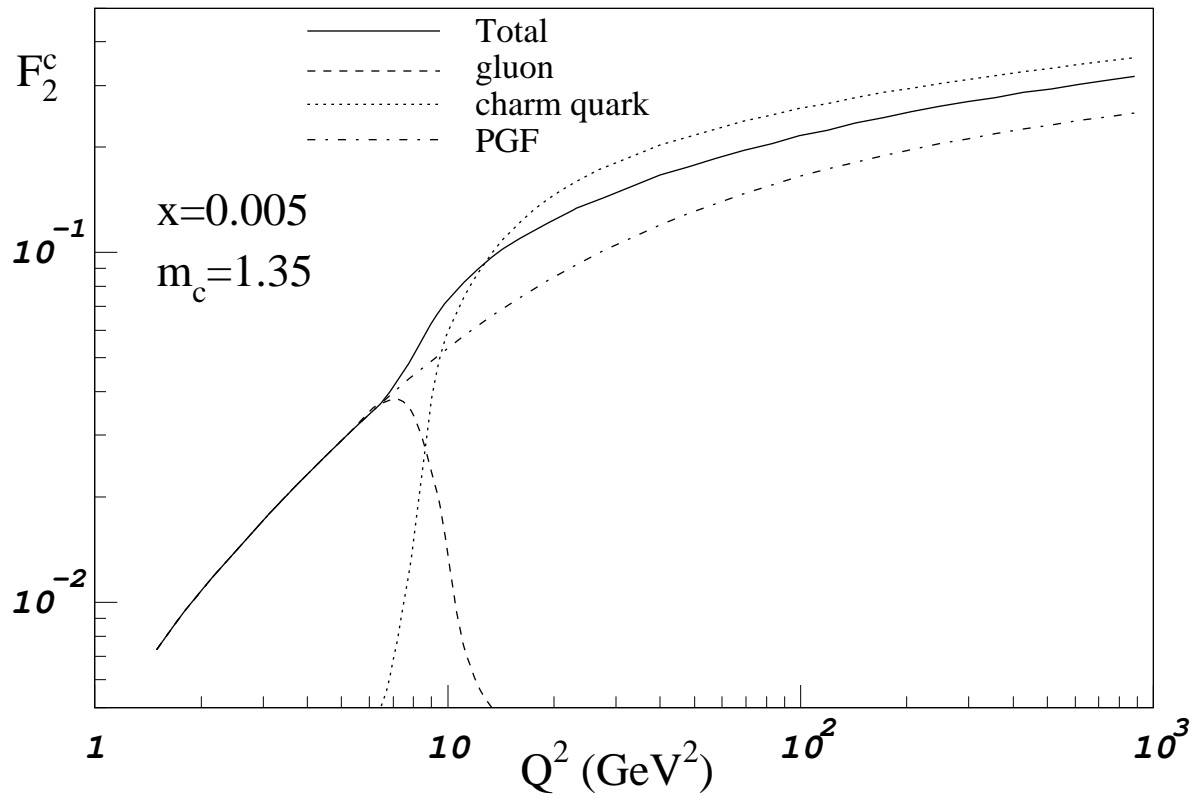


Fig. 6

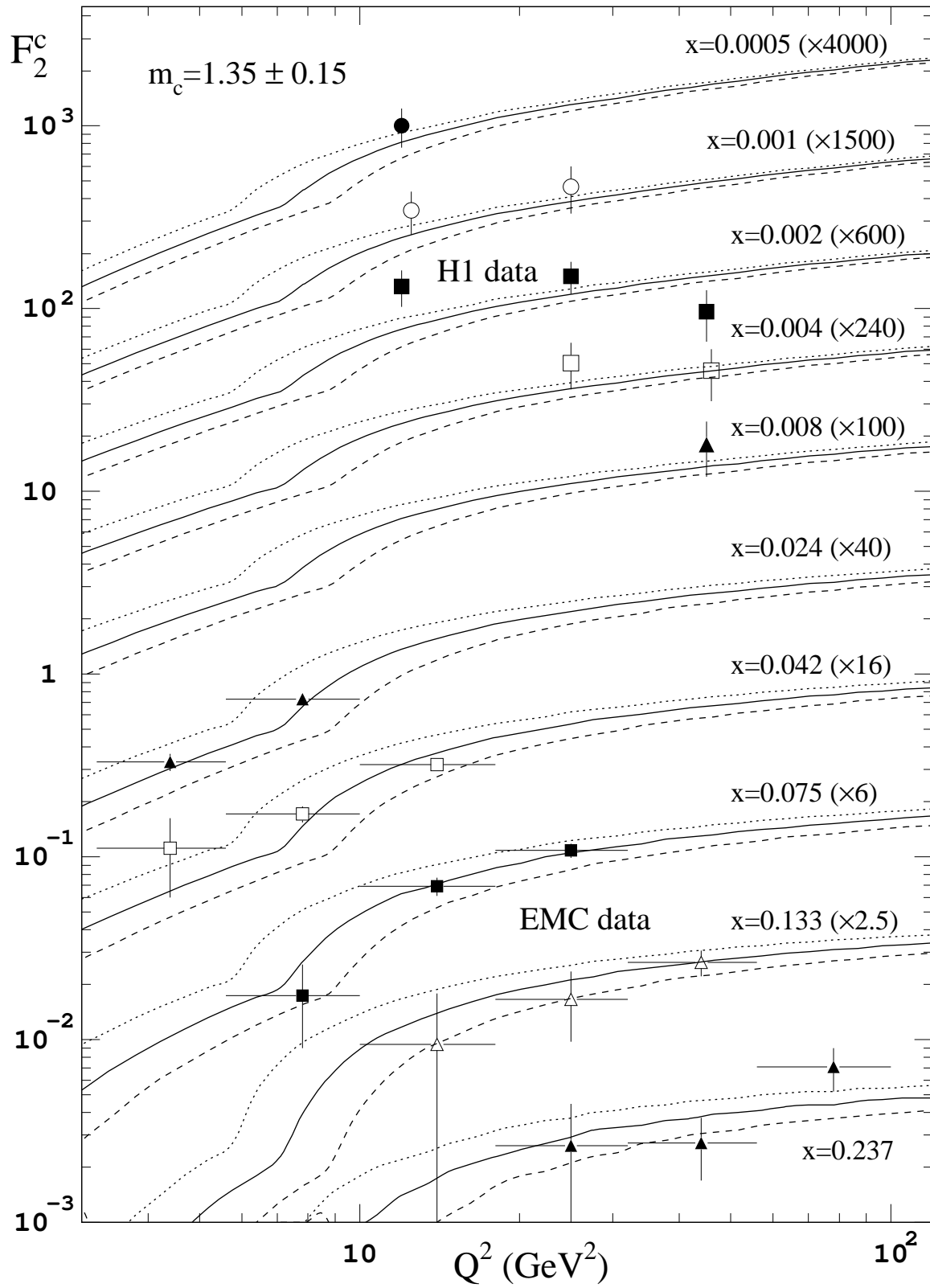


Fig. 7

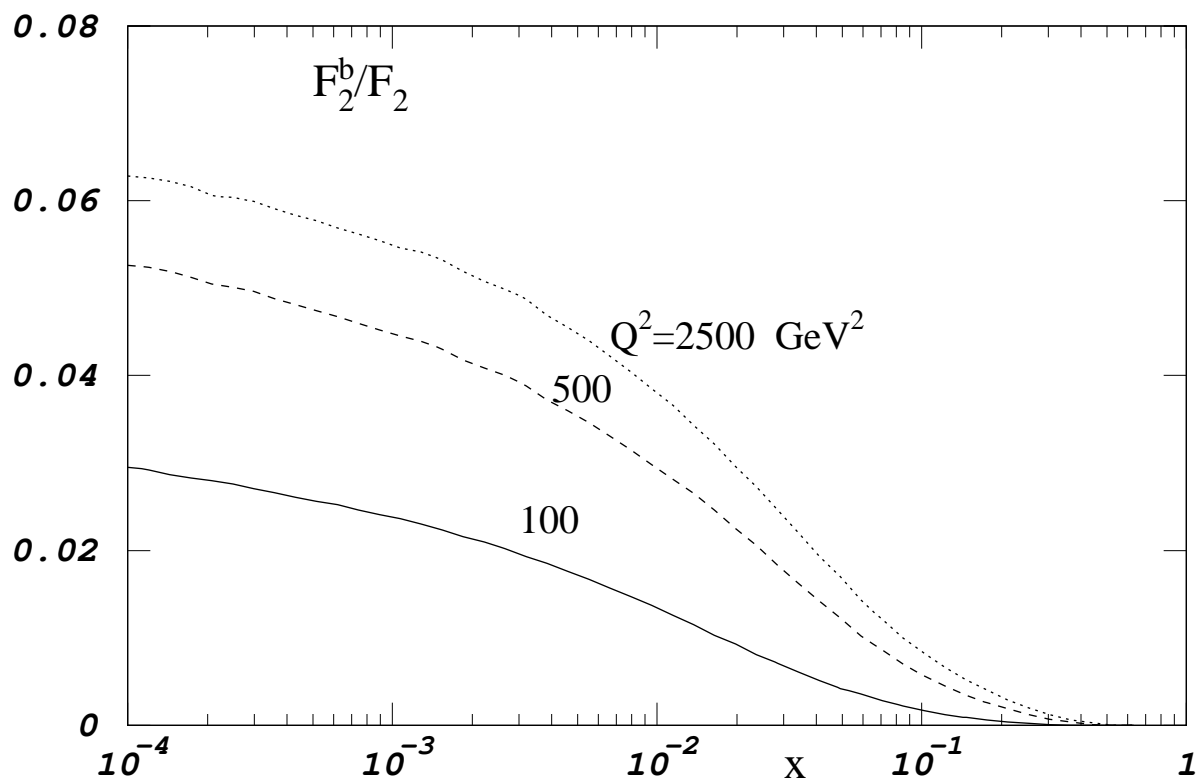
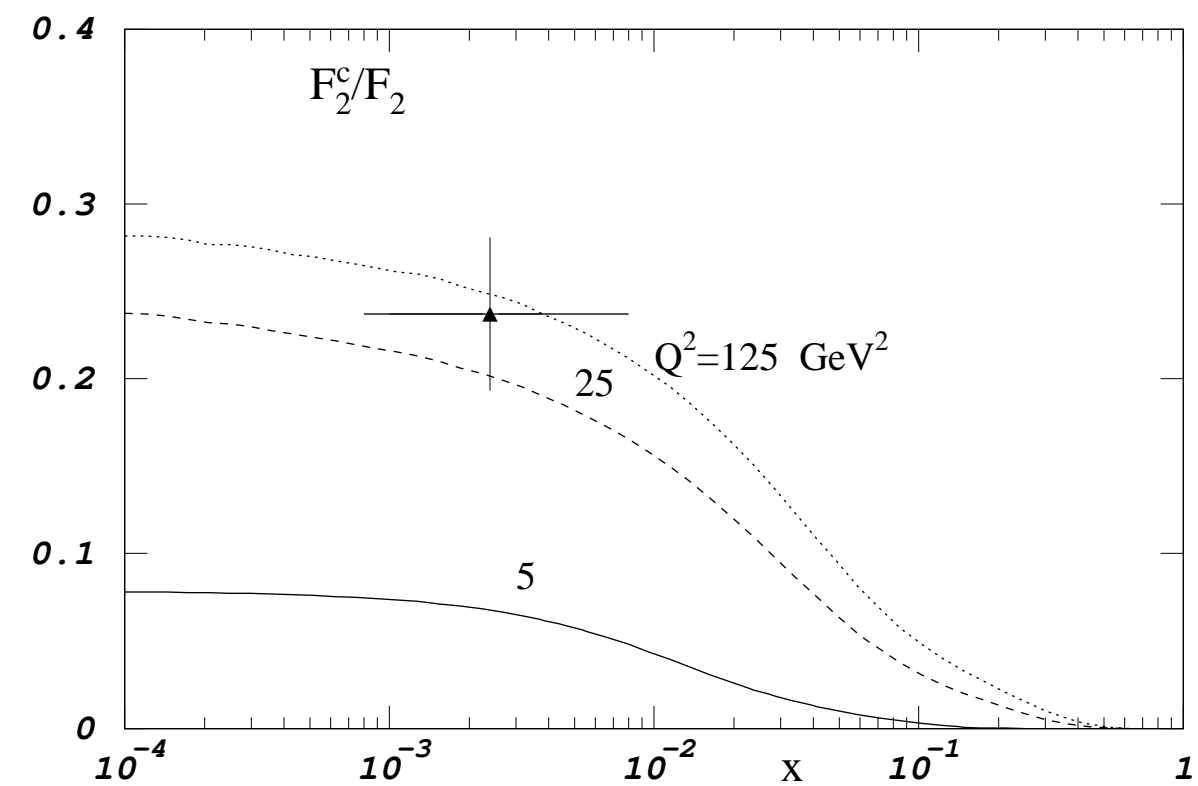


Fig. 8

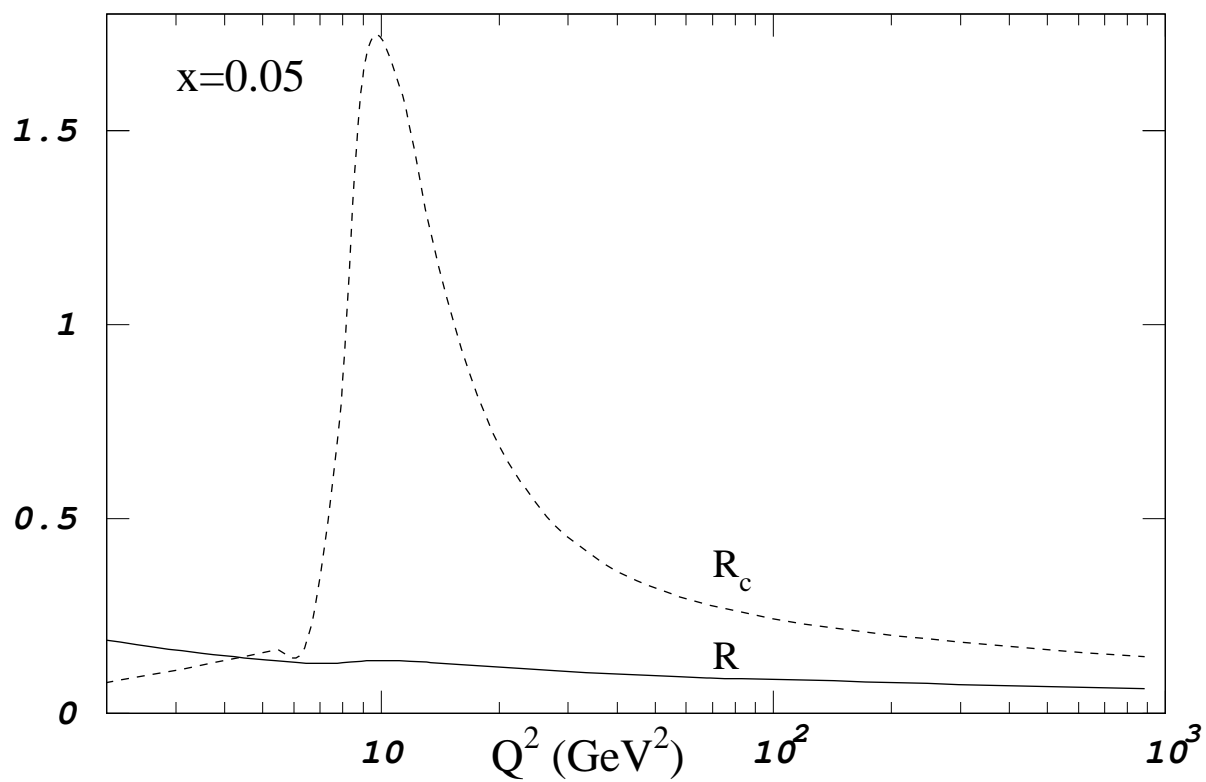
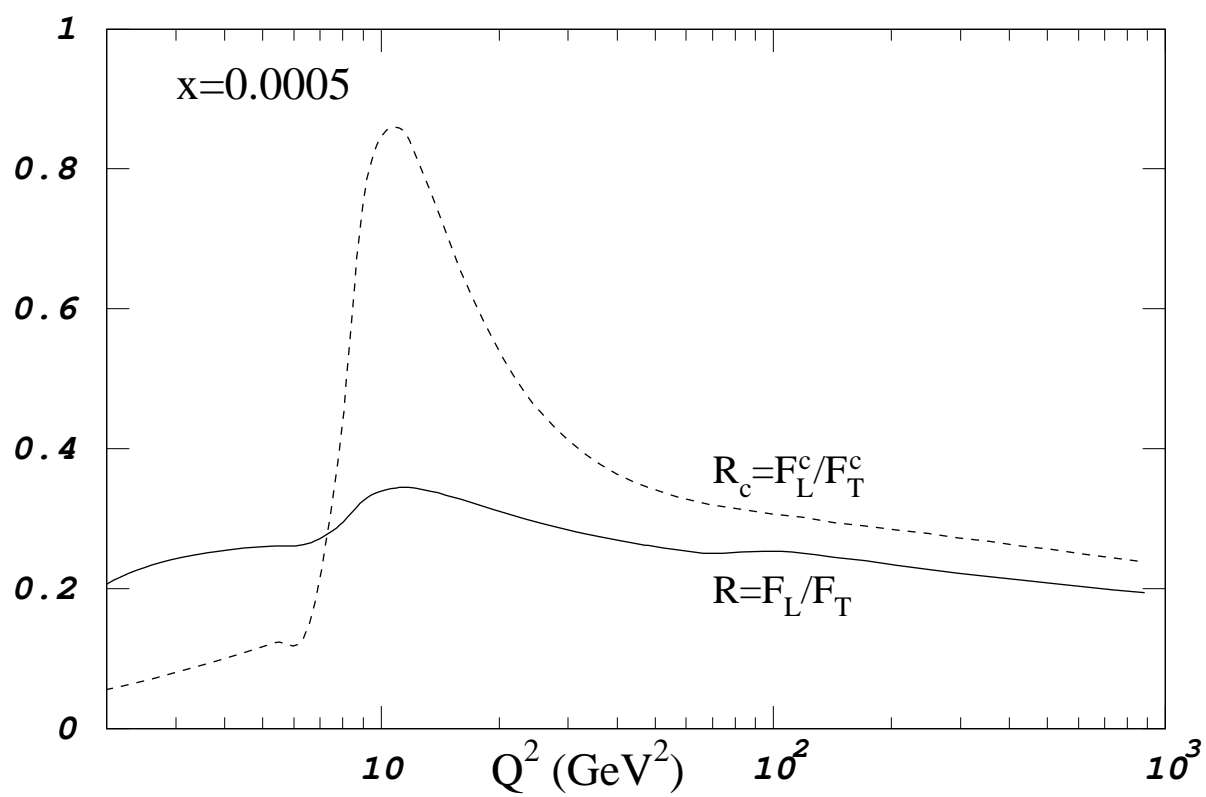


Fig. 9